The Cryosphere Discuss., 2, 777–810, 2008
www.the-cryosphere-discuss.net/2/777/2008/

The Cryosphere Discussions

The Cryosphere Discussions is the access reviewed discussion forum of *The Cryosphere*

Comparison of airborne radar altimeter and ground-based Ku-band radar measurements on the ice cap Austfonna, Svalbard

O. Brandt[1], R. L. Hawley[2,*], J. Kohler[1], J. O. Hagen[3], E. M. Morris[2], T. Dunse[3], J. B. T. Scott[4], and T. Eiken[3]

[1]Norwegian Polar Institute, Tromsø, Norway
[2]Scott Polar Research Institute, Cambridge, UK
[3]University of Oslo, Blindern, Norway
[4]British Antarctic Survey, Cambridge, UK
[*]now at: Dartmouth College, Hanover, NH, USA

Received: 15 September 2008 – Accepted: 22 September 2008 – Published: 3 November 2008

Correspondence to: O. Brandt (ola.brandt@npolar.no)

Published by Copernicus Publications on behalf of the European Geosciences Union.

Abstract

We compare coincident data from the European Space Agency's Airborne SAR/Interferometric Radar Altimeter System (ASIRAS) with ground-based Very High Bandwidth (VHB) stepped-frequency radar measurements in the Ku-band. The ASIRAS instrument obtained data from ~700 m above the surface, using a 13.5 GHz center frequency and a 1 GHz bandwidth. The ground-based VHB radar measurements were acquired using the same center frequency, but with a variable bandwidth of either 1 or 8 GHz. Four sites were visited with the VHB radar; two sites within the transition region from superimposed ice to firn, and two sites in the long-term firn area (wet-snow zone). The greater bandwidth VHB measurements show that the first peak in the airborne data is a composite of the return from the surface (i.e. air-snow interface) and returns of similar or stronger amplitude from reflectors in the upper ~30 cm of the subsurface. The peak position in the airborne data is thus not necessarily a good proxy for the surface since the maximum and width of the first return depend on the degree of interference between surface and subsurface reflectors. The major response from the winter snowpack was found to be caused by units of thin crust/ice layers (0.5–2 mm) surrounded by large crystals (>3 mm). In the airborne data, it is possible to track such layers for tens of kilometers. The winter snowpack lacked thicker ice layers. The last year's summer surface, characterized by a low density large crystal layer overlaying a harder denser layer, gives a strong radar response, frequently the strongest. The clear relationship observed between the VHB and ASIRAS waveforms, justifies the use of ground-based radar measurements in the validation of air- or spaceborne radars.

1 Introduction

Changes in mass and volume of glaciers and ice sheets are important contributors to rising global sea level (IPCC, 2007). Volume changes over Antarctica and Greenland are today routinely assessed by measuring surface elevation changes through

TCD

2, 777–810, 2008

time, using either radar or laser from air- or spaceborne platforms (Zwally et al., 2005; Thomas et al., 2006). Radar and laser both have advantages and disadvantages (Alley et al., 2007). A potential disadvantage of using radar is that the transmitted waves can penetrate several meters into snow, firn and ice before being reflected (Arthern et al., 2001; Lacroix et al., 2007). If the material properties change, over seasonal or longer time-scales, the degree of penetration can potentially vary as well (Scott et al., 2006a). Since radar altimeters have relatively large footprints, subsurface returns are merged with the return from surrounding surface topography. It can therefore be a challenge to actually pinpoint the surface elevation within the received waveforms (a process known as retracking), and measurements can be biased if not treated carefully. The accuracy of radar altimeters thus relies critically on characterization of subsurface returns and their temporal changes.

The topography in the interior of Greenland and Antarctica is relatively flat compared to the satellite radar footprint, so altimetric measurements from these areas are easier to interpret (Alley et al., 2007; Brenner et al., 2007). For ice sheet margins, outlet glaciers and ice caps, the topography is rougher and more seasonal and inter-annual changes are likely to occur. Near-surface changes include: formation of ice layers, lenses and glands as well as changes in free liquid water content and grain metamorphoses altering size and shape of crystals; all of which potentially alter the radar response. At Ku-band frequencies, typically used by altimeters, previous ground-based radar measurements have revealed large spatial and temporal variability in penetration and subsurface return (Jezek and Gogineni, 1992; Jezek et al., 1994; Scott et al., 2006a, b), with total backscatter composed of significant surface and subsurface (volume) backscatter components.

Ground-based radar measurements and in situ data are critical for validating air- (Kanagaratnam et al., 2007) and spaceborne radar instruments (Scott et al., 2006a, b; Langley et al., 2007) and have been used to relate airborne altimeter waveforms to subsurface properties. For example, Hawley et al. (2006) used the same airborne altimeter system discussed here to show that subsurface returns (down to ~10 m) from the dry

snow zone in Greenland correlate with firn density fluctuations. In a similar manner, Helm et al. (2007) showed that the Last Summer Surface (LSS) could be tracked within a profile recovered from the percolation zone to yield winter snow accumulation.

Here we compare coincident airborne altimeter waveforms with ground-based radar measurements and physical ground-truth. The data were retrieved in April–May 2007 from the superimposed ice (SI) and wet snow zone of the ice cap Austfonna, Svalbard, in an experiment designed to test and validate the European Space Agency's (ESA) planned space-borne CryoSat II radar altimeter. We apply the methods and ideas developed by Scott et al. (2006b), but expand on their work by presenting ground-based measurements alongside the airborne altimeter data. This enables us to directly confirm the frequently used assumption that ground-based radar measurements are a valuable tool for direct validation of the received waveforms from air- or spaceborne radars.

2 Test site

The Austfonna ice cap (79.7° N, 24.0° E) is one of the largest in the European Arctic, located on the island Nordaustlandet in the NE corner of the Svalbard archipelago. The ice cap is dome shaped and reaches to ~800 m a.s.l. Fig. 1, (Taurisano et al., 2007).

Air temperatures on Austfonna in summer typically remain above or around freezing (unpublished measurements from Etonbreen, Austfonna), which, combined with solar radiation causes melting, percolation and refreezing. In addition, melt and rain events can occur year round. The accumulation zone of Austfonna is therefore considered to be within the wet-snow zone as defined by Paterson (1994), and the firn is characterized by glands, lenses and ice layers, the latter ranging in thicknesses from millimeters to more than 0.5 m.

Repeated airborne laser altimetry measurements on Austfonna in 1996 and 2002 indicated a simultaneous elevation increase in the interior and a decrease at the margins (Bamber et al., 2004). Whether the elevation changes are driven by dynamic or

mass balance changes is still debated, and there is considerable uncertainty as to the current mass balance state of the ice cap (Pinglot et al., 2001; Taurisano et al., 2007; Schuler et al., 2007; Bevan et al., 2007; Dunse et al., 2008).

3 Data

3.1 Ground-based VHB radar

The ground-based radar is a stepped-frequency Very High Bandwidth (VHB) radar based on an Agilent network analyzer. Two wideband (2–18 GHz) horn antennas were mounted in HH mode pointing vertically downwards from an arm projecting 1.1 m from the side of a scooter sledge at a height of 1.15 m (bottom of antenna to snow surface). The radar was powered using a 3 kW Honda generator which was operated either on the snow surface or on an extra sled to avoid antenna movements due to engine vibrations. The system is described in detail by Scott et al. (2006b).

Field measurements were made from 2 to 18 GHz in 17 601 frequency steps with a step size of 909 kHz. The antenna radiation pattern and gain change to some extent over the frequency range. Therefore, following Scott et al. (2006b), during processing we limit the frequency range to have a bandwidth of 8 GHz with a center frequency of 13.5 GHz. For direct comparison with the airborne system, we also present data with the same center frequency but with a bandwidth of 1 GHz.

The range resolution ΔR depends on bandwidth and wave velocity v_ε in the medium according to Hamran et al. (1995):

$$\Delta R = \frac{v_\varepsilon}{2 \times \Delta F}. \quad (1)$$

Thus, for our 1 and 8 GHz bandwidths, the resolution in air is ΔR=0.15 and 0.019 m respectively. Nevertheless, if the area illuminated by a fine range resolution nadir looking radar is large, off-nadir returns may mask reflections from deeper layers and cause

clutter. This is schematically illustrated in Fig. 2. For a sufficiently coarse range resolution, off-nadir returns will arrive in the same range bin and clutter will not degrade later received range bins. Using the manufacturer's specified half-power beamwidth for the frequency range used, the illuminated area caused by the beamwidth is large compared to the range resolution ΔR for the 8 GHz bandwidth, resembling Fig. 2b. With the 1 GHz bandwidth, the range resolution is coarse enough that returns from off-nadir reflectors will not be as likely to cause clutter in later incoming range bins (Fig. 2a). Thus, in all of our measurements, clutter may limit the effective range resolution using the 8 GHz bandwidth. The degree to which the resolution is degraded due to clutter depends on several factors, including ray-bending in the subsurface, layer roughness and the type of scattering that dominates. An exact resolution, at which clutter will not significantly degrade the resolution, can therefore not be given quantitatively here, but the effect does not appear to significantly influence our results.

System background signals, caused by antenna feedbacks, cabling, or electronics, were evaluated by recovering traces with the antenna pointing upwards, and have subsequently been removed.

Following Langley et al. (2007), the received power P_R is converted to a weighted scattering cross section σ_w by correcting for the spherical spreading of the wave with distance R by:

$$\sigma_w = \frac{P_R R^4}{C V_S}, \tag{2}$$

where V_S is the volume sensed by each range bin, approximated as the illuminated area covered by the antenna beamwidth multiplied by the corresponding range resolution ΔR; fixed system factors such as antenna gain terms, wavelength and transmitted power are embedded in the constant C. The beamwidth as well as antenna gain varies with frequency, but the effect is small over the frequency range used and is therefore neglected (see Scott et al. (2006b) for thorough discussion).

Reflections in the radar data were correlated to stratigraphic units found in snow pits

by inserting an aluminium metal plate (0.3×0.3×0.003 m) into the pit walls wherever specific stratigraphic layers were observed. By comparing the signals received with and without the metal plate, the different major reflection sources could be determined. To reduce the influence of the snow-pit walls, antennas were offset typically 0.6 m from the edge of the pit.

3.2 ASIRAS

ESA's prototype Airborne SAR/Interferometric Radar Altimeter System (ASIRAS) was designed to reflect as closely as possible the characteristics of the SAR/Interferometric Radar Altimeter (SIRAL), which is the planned payload of CryoSat-II.

The ASIRAS instrument is a linear frequency-modulated synthetic aperture radar with a 13.5 GHz center frequency and 1 GHz bandwidth (Lentz et al., 2002; Hawley et al., 2006). For this field campaign, the ASIRAS was operated in low-altitude-mode at typical elevations of ∼700 m above the surface. The positioning of the profiles was done by Differential Global Positioning System (DGPS) and an Inertial Navigation System (INS). The elevation is relative to the geodetic ellipsoid, WGS84. Profile cross-over points were used to verify data replicability. Some of the profiles were found to have a low waveform correlation, presumably due to rapid and high amplitude aircraft movements (Helm et al., 2007), and have been discarded. The ground spacing between each trace recorded by ASIRAS depends on aircraft speed relative the ground, but is typically 8–10 m after post-processing.

Raw data were post-processed using the ESAs' ASIRAS L1b processor. The processor uses delay-doppler to focus the beam in the along-track direction, giving it an effective footprint of ∼5×50 m (along- versus across-track). Speckle and thermal noise is further reduced by multi-looking (Wingham et al., 2004), and finally, the echo waveforms are geo-located using the DGPS and INS. After processing the raw data, each trace is built up of 4048 samples, in which each range bin equals 0.1097 m in air. In the profiles presented here, this range bin distance has been corrected to compensate for the lower wave velocity in the snow, to give a correct depth scale at least down to

the LSS.

The surface has been tracked using a simple but robust threshold re-tracker. The threshold re-tracking point was set to 20% of the average maximum peak amplitude in the profile. Traces with a significantly lower peak maximum power compared to the rest of the profile (<2 × threshold) have been discarded. In a few traces the 20% re-tracking point has changed unrealistically in position, i.e. giving unrealistic changes in surface elevation or air craft height in between traces. In these situations, 10% local threshold was used instead. If unrealistic position changes remained, the trace has been discarded. After surface re-tracking, the data has been corrected for elevation and aircraft height variations to give a depth scale starting at zero at the re-tracked surface position bin.

3.3 Snow pits

Snow pits were excavated down to the LSS, or occasionally ~0.5 m deeper. The pits were logged for density (by measuring the weight of bulk samples), temperature, visual snow stratigraphy and mean snow crystal size. To compare the wave velocity determined using the VHB radar (see below), the density ρ (kg m^{-3}) has been converted to relative permittivity following Kovacs et al. (1995):

$$\varepsilon_r = \left(1 + 8.45 \times 10^{-4}\rho\right)^2. \quad (3)$$

The relative permittivity ε_r is then converted to wave velocity using:

$$v_\varepsilon = c/\sqrt{\varepsilon_r}, \quad (4)$$

where c is the speed of light (~3×10^8 m s^{-1}).

3.4 Neutron probe

Access holes for the neutron probe were drilled using a Kovacs auger with a diameter of ~5 cm. During drilling, the auger was guided by a 1-m long aluminium tube inserted into

the snow, ensuring that the holes were vertical and minimizing variations in diameter in the softer upper snow layers.

The neutron probe contains a radioactive source that emits fast neutrons. These lose energy by scattering in the snow (mainly from hydrogen nuclei) and the number of slow neutrons arriving back to a boron trifluoride detector in the probe are counted. The number of returning slow neutrons is related to density, hole diameter and the position of the probe relative to the wall (Hawley and Morris, 2006; Morris, 2008).

The probe was lowered to the bottom of the access hole and then raised to the surface while logging, at a speed of $\sim 3\,\mathrm{m\,hr^{-1}}$. The relatively low speed allows sufficient time at each depth to average out random fluctuation in the count rate caused by random variations in the number of neutrons emitted over time by the radioactive material. The number of slow neutrons is counted over a time period of 100 ms and is averaged out over the time it takes for the probe to move 1 cm (~12 s), such that the record has a nominal resolution of ~1 cm. However, thin ice layers and abrupt density changes are not fully resolved. They appear smoothed over slightly greater length scales (Hawley et al., 2008), in part because neutrons are scattered over a finite volume of snow, and more importantly because the detector used has an active length of 13.5 cm. The density is then calculated from the neutron record using the calibration method outlined by Morris (2008).

4 Electromagnetic velocity estimates

In the winter snow, the wave velocity was estimated directly by positioning the VHB radar (8 GHz bandwidth) close to the edge of the pit and inserting the metal plate in the wall, starting from the bottom and finishing up at the surface. The velocity is then obtained from time differences between the reflections from the surface and the metal plate, and the measured depth of the plate (Fig. 3). Error bars are calculated based on a ±0.025 m depth uncertainty in the placement of the metal plate.

There is a good agreement between VHB-estimated wave velocities and those

calculated from bulk density measurements in the snow pit (Eqs. 3 and 4). The radar-measured velocities obtained below 1 m are $\sim 2.28\times10^8 \pm 0.08\times10^8$ m s^{-1}, while typical pit bulk densities were 400 ± 25 kg m^{-3}, equivalent to a wave velocity of $2.24\times10^8 \pm 0.04\times10^8$ m s^{-1}. In the following calculations we have therefore used a speed of 2.28×10^8 m s^{-1} for all conversions between depth and radar travel time.

The empirical relation (Eq. 3) is valid for dry snow and firn. This condition was certainly fulfilled during the measurement period, with temperatures in the snow ranging from -23°C at the surface to -8°C close to the LSS.

5 ASIRAS and VHB radar comparison

5.1 Site "cry1"

The site is located (Fig. 1) at the border between the long-term firn and SI zone, in an area in which the firn line has migrated back and forth over the last years (Dunse et al., 2008). The site has a thin ~1 m firn layer superimposed on older accumulated SI (Fig. 4a).

The ground-based VHB radar data are shown together with the snow pit and neutron probe data in Fig. 4. The 8 GHz bandwidth data show that the near surface reflections (Fig. 4, labeled "(2)") correspond in depth with units of large crystals and thin crust/ice layers at depths of ~8, 27 and 29 cm and are of equal strength to the air-snow surface reflection marked (1) in Fig. 4. Units of low density comprising large crystals (not resolved in the bulk density profile (Fig. 4a)) were observed without crust or ice layers at ~75 cm depth and give rise to detectable reflections (Fig. 4, "(3)"). At ~1 m depth a 1 mm crust/ice layer overlaying a thin large crystal layer was observed in the pit. This layer varied significantly in depth along the pit walls and is detected only sporadically by the VHB radar. The weak radar response could be due to the depth variability of the layer, or alternately, the size of the layer might not be spatially homogeneous. The LSS at this site is a unit of large crystals on an ice layer situated atop firn. In the radar data

the LSS is represented by a sharp increase in backscatter (Fig. 4, "(4)"). Below the LSS the radar backscatter is typically −22 to −18 dB over a 5 ns band, and originates from the firn (Fig. 4, "(5)"). Within this band more spatially continuous reflection horizons are occasionally observed, which we attribute to thin (3–10 mm) ice layers. These reflections often reach up to −10 dB and are thus ∼10 dB stronger relative to the high backscatter band.

At this site the VHB data coincides well with two airborne ASIRAS profiles (Fig. 5). The profiles comprise three major reflecting horizons, with the lower having the highest amplitude. The first horizon has a peak amplitude of ∼75% compared to the lowermost, while the middle horizon has about ∼25%.

The ASIRAS and VHB radar responses compare well despite different profile lengths (Fig. 6); as with the VHB, the strongest response in the ASIRAS data is from the LSS. The surface and near surface returns (0–30 cm), which are apparent in the 8 GHz bandwidth VHB radar data, merge into a single reflection when the bandwidth is reduced to 1 GHz (Fig. 6b). Thus, in the ASIRAS data, the first returned peak is a convolution of the air-snow interface and the often stronger reflections from the upper ∼30 cm. The internal reflection from the winter snowpack comes from the same depth range (∼75 cm) as a sequence of layers built up of large crystals (>3 mm in diameter).

5.2 Site "cry2"

This site is within the long-term firn area (Fig. 1). At a depth of ∼5 m and below, the firn is characterized by 10–50 cm thick ice layers. The layers continue to a depth of at least 8 m, the deepest neutron record at this site.

The VHB data is characterized by a strong surface return (Fig. 7b, labeled "(1)"). This reflected energy comes from the air-snow interface and a sharp increase in density below a 0–2 cm low-density surface powder snow. At ∼2.2 ns a reflection was observed (Fig. 7b, "(2)"), coinciding with the depths of two thin ice crust layers at 25 and 27 cm. Typically these reflections have the same or stronger amplitude than the air-snow surface return. Two other significant reflection horizons are seen at ∼5 and 8 ns (Fig. 7b,

"(3)"), corresponding in depth with a sequence of thin ice layers/crusts, both underlain by large crystals (3–4 mm diameter).

The LSS, here characterized by a low density large crystal layer (~5 cm thick) on top of a weak densification, is detected in the VHB data as an abrupt increase in backscatter (Fig. 7b, "(4)"). Below the LSS, the firn matrix, made-up of large crystals and comprising a significant number of melt features such as ice pipes and lenses, is responsible for the high backscatter (typically −25 dB) (Fig. 7b, "(5)"). At a depth of 2.25 m, multiple thin ice layers (spatially continuous in the pit as opposed to the lenses) interrupt the firn (and the backscatter rich band). These layers correspond well to the vaguely visible but more spatially continuous reflection horizon (−20 to −15 dB) at a 20 ns depth in the radar data.

The airborne profile 1 coincides well with the ground-based profile and the corner reflector is detected (Fig. 8). Like the VHB data, the ASIRAS waveform is characterized by a strong surface or near surface return. This return is followed by two returns with typically 50–60% lower amplitude.

The ASIRAS data and the VHB radar data are shown together in Fig. 9. Similarly to "cry1", we find that the two surface returns, at ~0 and ~2 ns respectively in the 8 GHz bandwidth data, merge to one horizon when imaged with the 1 GHz bandwidth data. The same happens for the two reflections from the interior of the winter snow-pack (at ~5 and ~8 ns). Despite differences in amplitude of the two lower reflections, likely a result of the short VHB profile length (15 m) giving a poor spatial representation, the air and ground-based waveforms compare well.

5.3 Site "camp07"

The "camp07" site is also within the long-term firn area, but differs from "cry2" at depths below 3.5 m. The firn is characterized here by ice layers (10—40 cm thick). Ice with no or very little firn starts at a depth of ~6 m and continues down to at least 14 m, where the deepest neutron probe record ends.

At this site two 100 m VHB radar profiles were retrieved. In Fig. 10, one of the profiles

is shown together with ground truth data. Typically, the strongest return stems from the air-snow interface (Fig. 10b, labeled "(1)") and a thin crust layer accompanied by a sharp increase in snow hardness and density (the density contrast is not resolved in Fig. 10a due to the coarse bulk sample size). A thin crust layer at 38 cm depth in the snow pit, but varying in depth along the profile, was also found to give a significant near surface waveform contribution (Fig. 10b, "(2)"), despite it being spatially discontinuous along the profile. For example, in the middle of the profile, at a distance of ∼50 m, this layer nearly reaches the surface. Below this layer several units of crust/ice layers imbedded in large crystals give rise to several individual reflecting horizons.

The VHB return from the LSS is characterized at "camp07" by a gradual increase in backscatter with depth (Fig. 10b, "(3)"), unlike the other sites where a more abrupt increase in backscatter was found. We note that at this site a thicker (relative to the other sites) low density layer of large crystals on top of the LSS hard/dense layer were observed. The snow pit was not extended below the LSS and we therefore do not have information regarding the firn makeup.

"Camp07" was the site where most VHB data was obtained; unfortunately, the ASIRAS data is sparse at this site due to many discarded traces, furthermore, there is a significant spatial offset between the ground and airborne measurements here, both of which prohibit a reasonable comparison between the data sets.

5.4 Site "coreF"

This site, like "cry1", lies at the border between the long-term firn area and the SI area (Fig. 1), and similarly to "cry1", the SI at this site was overlaid by a <1 m thick firn layer.

The surface VHB radar return comes from the same depth range as the relatively hard air-snow interface (Fig. 11b, labeled "(1)") and a sequence of two thin crust/ice layers at ∼24 and 34 cm depth (Fig. 11b, "(2)"). At a depth of ∼62 and 64 cm, two closely spaced crust/ice layers surrounded by low density large crystals correspond well with a reflection at ∼6 ns (Fig. 11b, "(3)"). A low density layer at 89–97 cm depth, comprising crystals with a typical diameter of 3 mm, corresponds to a reflection at ∼8

ns but appears from the radar profile to have a relatively limited spatial extent (Fig. 11b, "(4)").

The LSS at this site is seen as a clear and abrupt reflection horizon (Fig. 11b, "(5)") followed by a backscatter rich band (Fig. 11b, "(6)"), the latter caused by the firn matrix; here characterized by large crystals and refrozen melt features such as ice lenses, layers and pipes. Within this band, more spatially well-defined reflection horizons are seen, which we attribute to thin ice layers imbedded in the firn. These reflections reach up to −10 dB, while the backscatter band typically reaches between −25 to −20 dB. These observations correspond well with those at "cry1", which has much the same glaciological setting. Below the backscatter rich band, at ∼24 ns (Fig. 11b, "(7)") another band of higher backscatter is detected. This band is connected to the transition from the firn to SI, but we do not have any information about fine scale layering or typical crystal sizes at this depth.

As at the "camp07" site, large portions of the ASIRAS data were discarded and were spatially offset from the ground measurements, prohibiting a side-by-side comparison. Nevertheless, the nearest ASIRAS data (∼800 m away) show that the strongest returns are connected to the surface and LSS, with the latter of more consistent strength compared to returns from the surface and winter snowpack (Fig. 12). This resembles closely the same characteristics of the VHB data but due to the spatial offset limited conclusions can be drawn.

6 Results from ASIRAS and VHB radar comparison

At the two sites where the VHB and ASIRAS data coincide spatially, a good comparison is found between the ground and airborne data, implying that ground-based measurements are a valuable tool for direct validation and improved information extraction from air- or spaceborne measurements.

The VHB radar data shows that the major response from the winter snow pack at Ku-band frequencies are connected to:

1. Units of thin crust or ice layers (0.5–2 mm thick) surrounded by low density layers builtup of large crystals, typical diameter >3 mm. The snow pack lacked thicker ice layers and therefore we cannot deduce the radar response of such layers.

2. Medium to weak reflections may be caused by a low density layer built up of large crystals or a crust layer alone, but the two combined seems to give the strongest response observed.

3. These backscatter sources (1 and 2) give rise to reflections from within the winter snowpack that are trackable for several tens of kilometers in the airborne data.

4. The radar response from the air-snow interface is typically of a similar amplitude to thin subsurface layers which can be found frequently in the top 30 cm of the winter snow pack. At narrower bandwidths (e.g. 1 GHz) these reflections merge, and thus the maximum peak position is not a good surface proxy. The offset from the true surface depends on the degree of interference between the air-snow interface and the backscatter from the near surface layers.

The LSS was characterized at all sites by a low density large crystal layer overlaying a harder, denser layer of variable thickness, which in turn was situated over firn. This sequence gives a strong response at all sites, strongest in the SI-firn transition zone and weaker in the long-term firn area. It has not been possible to quantify the importance (in reflection power) of the low density large crystal layer relative to the dense layer due to the small depth separation and the few sites visited.

Below the LSS, the firn is typically characterized by large crystals (>3 mm) and refrozen melt intrusions such as ice layers, lenses and glands. This is seen in the VHB data as a ∼5 ns backscatter rich band, typically reaching a signal strength of −25 to −20 dB. Within this band, fairly well defined reflection horizons (often up to −10 dB) are found associated with thin ice layers with thicknesses larger than ∼2–3 mm. This is particularly evident at the “coreF” site.

The deepest observed coherent reflections, stronger than the surrounding clutter, were found within the SI-firn boundary zone at a depth of roughly 4 m. In the long-term firn area the deepest observed reflections are at ∼3 m depth. In the ASIRAS data the depth penetration is limited to just below the reflection connected to the LSS. Occasionally deeper reflectors (both within the SI and firn area) are seen, but we lack ground-truth and cannot pinpoint the source in those places.

7 Discussion

7.1 Clutter and reflection sources

Off-nadir reflections causing clutter may degrade the range resolution of the VHB radar, especially using the 8 GHz bandwidth. Despite the fine range resolution we can therefore not exactly determine the individual contribution of closely spaced stratigraphic units, such as layers of low bulk density built up of large crystals relative to high density stratigraphic layers such as crusts or ice layers. This is likely better determined using numerical modeling or controlled laboratory experiments. It is nevertheless clear from both the ground and airborne data, that the strongest reflections in the winter snow pack originate from thin dense layers surrounded by large crystals. The influence of the large crystal layers on the response is likely that they form a less dense layer compared to the surrounding snow, creating an increased permittivity contrast. Unfortunately, due to the large bulk sizes used to measure the density and the smearing occurring in the neutron probe data, accurate measurements of the large crystal layers density (alone) is not available. There may be some minor scattering for 3 mm crystals, but with a wavelength close to 20 mm in the winter snowpack, this will not be significant.

7.2 LSS response

In the long-term firn area, the LSS response appears weaker compared to sites within the SI-firn transition zone. The difference in LSS power and waveform shape could potentially be used to delineate different glacier zones or facies from each other. This remains to be demonstrated though, since the difference is not only caused by the less developed LSS densification but is also related to varying attenuation due to changes in winter snow pack thickness, as well as to the degree a low density large crystal layer increases the permittivity contrast or causes constructive or destructive interference with the dense layer response.

7.3 Re-tracker and elevation correction

Using the VHB radar the air-snow interface return is easily identified by laying a metal plate on the surface. Reducing the bandwidth to 1 GHz during post-processing yields a "surface" waveform which is a convolution of the air-snow interface reflection and reflections from within the upper ~30 cm of the winter snowpack. From the high bandwidth data, we see that the latter are typically of the same magnitude or stronger. Because the return maximum power and shape is merely a function of interference between the closely spaced reflectors (layers within the snow pack and the air-snow boundary), we believe that most information about the air-snow interface is found in the leading edge of the response, and to a lesser extent related to the peak power or width of the "surface return". This might not necessarily be true over areas where the surface is rougher, but is found to be the case at our field sites where the surface had a typical small scale roughness, subjectively determined along the ground profiles to be less than 0.25 m.

We found that tracking the leading edge of the first peak using a 20% threshold relative the typical maximum power in the ASIRAS data gives a reasonable proxy for the air-snow interface when compared to the VHB data. This may not always be the best method, but it is likely to be a good choice at many sites due to the frequently

strong near-surface reflections which interfere with the air-snow interface response.

8 Conclusions

We have compared ground- (VHB) and airborne (ASIRAS) radar altimeter data over the Austfonna ice cap, Svalbard. Snow pits and neutron probe density profiles have been used to ground-truth the data. Two sites were situated in the long-term wet-snow zone firn area and two in the SI-firn transition zone.

We find that the ASIRAS waveforms compare well with the ground-based VHB radar measurements, implying that ground-based radar measurements are a valuable tool for direct validation and improving information extraction from air- or spaceborne measurements.

Over the accumulation area of the ice cap three reflecting horizons are typically found in the airborne data. From VHB measurements the reflections are attributed as follows:

1. The first return in the airborne data is a composite of the surface return (i.e. air-snow interface) and reflections from the upper ~30 cm of the subsurface. The 8 GHz bandwidth data show that reflections from just below the air-snow interface were as strong, or stronger, than the surface reflection. In the airborne data the maximum amplitude and width of the return is therefore dependent on the degree of interference of the air-snow interface and near surface returns. Hence, we believe most of the air-snow interface information is, at low slope and roughness sites, stored in the leading edge of the returned waveform. We have therefore chosen to use a robust and simple 20% threshold re-tracker, to obtain a good correspondence with the ground-based radar measurements.

2. We found that within the winter snowpack, units of low density layers built up of crystals larger than ~3 mm surrounding thin crusts or ice layers less than ~2 mm thick give rise to the strongest backscatter. Such layers are clearly seen in the

airborne data and give rise to reflections trackable for several tens of kilometers. Layers of low density large crystals or crust and ice layers alone, do give a detectable backscatter contribution, but the amplitude of the radar response is weaker. Nevertheless, such layers can still be tracked in the airborne data for considerable distances. The large crystals alone may cause minor scattering, but it is likely that the major response is caused by the layer being of lower density compared to the surrounding snow. The snow pack lacked thicker ice layers and therefore we cannot judge the response to such layers.

3. LSS gave in all cases a strong response, frequently the strongest – but appears to be weaker at the long-term firn area sites. The difference in power and shape of the LSS reflection could therefore potentially be used to delineate glacier facies using altimeter waveforms.

Below the LSS, the VHB radar data is characterized by a band of higher backscatter. The band is typically about 5 ns deep before it drops off to the noise threshold. This higher backscatter originates from the firn which is characterized by large crystals (typical diameter >3–4 mm) and refrozen melt intrusions in the form of ice lenses and layers as well as glands. The response to the thicker ice layers are revealed as more well-defined reflecting horizons, which can be readily tracked horizontally as single discrete layers within the clutter-rich band.

Our findings using the VHB radar on Austfonna confirm the results from previous ground-based Ku-band radar measurements (Scott et al., 2006b, a), as well as the interpretations made by Helm et al. (2007) using the ASIRAS altimeter in the Greenland percolation zone. Furthermore, here we validate the frequently used assumption that ground-based radar measurements can be directly related to waveforms retrieved by airborne radars, justifying their use as a means of calibration for future missions such as ESA's CryoSat II radar altimeter.

Acknowledgements. This work was supported by European Space Agency (ESA), the Norwegian Space Center, and the Norwegian Research Council (IPY project GLACIODYN). The authors are grateful to all who were involved in the CryoVEx 2007 Svalbard activities.

References

Alley, R. B., Spencer, M. K., and Anandakrishnan, S.: Ice-sheet mass balance: assessment, attribution and prognosis, Ann. Glaciol., 46, 1–7, 2007.

Arthern, R. J., Wingham, D. J., and Ridout, A. L.: Controls on ERS altimeter measurements over ice sheets: footprint-scale topography, backscatter fluctuations, and the dependence of microwave penetration depth upon satellite orientation, J. Geophys. Res., 106(D24), 471–484, 2001.

Bamber, J., Krabill, W., Raper, V., and Dowdeswell, J.: Anomalous recent growth of part of a large Arctic ice cap: Austfonna, Svalbard, Geophys. Res. Lett., 31, L12402, doi:10.1029/2004GL019667, 2004.

Bevan, S., Luckman, A., Murray, T., Sykes, H., and Kohler, J.: Positive mass balance during the late 20th century on Austfonna, Svalbard, revealed using satellite radar interferometry, Ann. Glaciol., 46, 117–122, 2007.

Brenner, A. C., DiMarzio, J. P., and Zwally, H. J.: Precision and Accuracy of Satellite Radar and Laser Altimeter Data Over the Continental Ice Sheets, IEEE Trans. Geosci. Remote Sens., 45, 2, 321–331, 2007.

Dunse, T., Schuler, T. V., Hagen, J. O., Eiken, T., Brandt, O., and Høgda, K. A.: Recent fluctuations in the extent of the firn area of Austfonna, Svalbard, inferred from GPR, Ann. Glaciol., in press, 2008.

Hamran, S.-E., Gjessing., D. T., Hjelmstad, J., and Aarholt, E.: Ground penetrating synthetic pulse radar: dynamic range and modes of operation, J. Appl. Geophys., 33, 7–14, 1995.

Hawley, R. L., Morris, E. M., Cullen, R., Nixdorf, U., Shepherd, A. P., and Wingham, D. J.: ASIRAS airborne radar resolves internal annual layers in the dry-snow zone of Greenland, Geophys. Res. Lett., 33, L04502, doi:10.1029/2005GL025147, 2006.

Hawley, R. L. and Morris, E. M.: Borehole optical stratigraphy and neutron-scattering density measurements at Summit, Greenland, J. Glaciol., Instruments and Methods, 52, 179, 491–496, 2006.

Hawley, R. L., Brandt, O., Morris, E. M., Kohler, J., Shepherd, A. P., and Wingham, D. J.: Techniques for measuring high-resolution firn density profiles: case study from Kongsvegen, Svalbard, J. Glaciol., Instruments and Methods, 54, 186, 463–468, 2008.

Helm, V., Rack, W., Cullen, R., Nienow, P., Mair, D., Parry, V., and Wingham, D. J.: Winter accumulation in the percolation zone of Greenland measured by airborne radar altimeter, Geophys. Res. Lett., 34, L06501, doi:10.1029/2006GL029185, 2007.

IPCC: Contribution of working group i to the fourth assessment report of the intergovernmental panel on climate change, in: Climate Change 2007: The Physical Science Basis., edited by: Solomon, S., Qin, D., Manning, M., Chen, Z., Marquis, M., Averyt, K., Tignor, M., and Miller, H., Cambridge University Press, Cambridge, United Kingdom and New York, NY, USA, 2007.

Jezek, K. and Gogineni, S.: Microwave remote sensing on the Greenland ice sheet, IEEE Geoscience and Remote Sensing Society Newsletter, 9, 6–10, 1992.

Jezek, K. C., Gogineni, P., and Shanableh, M.: Radar measurements of melt zones on the Greenland ice sheet, Geophys. Res. Lett., 21, 33–36, 1994.

Kanagaratnam, P., Markus, T., Lytle, V., Heavey, B., Jansen, P., Prescott, G., and Gogineni, S. P.: Ultrawideband Radar Measurements of Thickness of Snow Over Sea Ice, IEEE Trans. Geosci Remote Sens., 45, 9, 2715–2724, 2007.

Kovacs, A., Gow, A. J., and Morey, R. M.: The in situ dielectric constant of polar firn revisited, Cold Reg. Sci. Technol., 23, 3, 245–256, 1995.

Lacroix, P., Legrésy, B., Coleman, R., Dechambre, M., and Rémy, F.: Dual-frequency altimeter signal from Envisat on the Amery ice-shelf, Remote Sens. Environ., 109, 3, 285–294, 2007.

Langley, K., Hamran, S.-E., Høgda, K.-A., Storvold, R., Brandt, O., Hagen, J.-O., and Kohler, J.: Use of C-Band Ground Penetrating Radar to Determine Backscatter Sources Within Glaciers, IEEE Trans. Geosci. Remote Sens., 45, 5, 1236–1246, 2007.

Lentz, H., Braun, H.-M., Younis, M., Fletcher, C., Wiesbeck, W., and Mavrocordatos, C.: Concept and realization of an airborne SAR/ Interferometric Radar Altimeter System (ASIRAS), IGARSS '02, Inst. Electr. Electr. Eng., New York., 6, 3099–3101, 2002.

Morris, E. M.: A theoretical analysis of the neutron scattering method of measuring snow and ice density, J. Geophys. Res., 113, F03019, doi:10.1029/2007JF000962, 2008.

Paterson, W. S. B.: The physics of glaciers. Third Edition. Pergamon, Elsevier Science, Oxford, UK, ISBN 0-08-037944-3, 1994.

Pinglot, J. F., Hagen, J. O., Melvold, K., Eiken, T., and Vincent, C.: A mean net accumulation

pattern derived from radioactive layers and radar soundings on Austfonna, Nordaustlandet, Svalbard, J. Glaciol., 47, 159, 555–566, 2001.
Schuler, T. V., Loe, E., Taurisano, A., Eiken, T., Hagen, J.-O., and Kohler, J.: Calibrating a surface mass-balance model for Austfonna ice cap, Svalbard, Ann. Glaciol., 46, 241–248, 2007.
Scott, J. B. T., Nienow, P., Mair, D., Parry, V., Morris, E., and Wingham, D. J.: Importance of seasonal and annual layers in controlling backscatter to radar altimeters across the percolation zone of an ice sheet, Geophys. Res. Lett., 33, L24502, doi:10.1029/2006GL027974, 2006a.
Scott, J. B. T., Mair, D., Nienow, P., Parry, V., and Morris, E.: A ground-based radar backscatter investigation in the percolation zone of the Greenland ice sheet, Remote Sens. Environ., 104, 361–373, 2006b.
Taurisano, A., Schuler, T. V., Hagen, J.-O., Eiken, T., Loe, E., Melvold, K. and Kohler, J.: The distribution of snow accumulation across Austfonna ice cap Svalbard: direct measurements and modeling, Polar Res., 26, 1, 7–13, 2007.
Thomas, R., Frederick, E., Krabill, W., Manizade, S., and Martin, C.: Progressive increase in ice loss from Greenland, Geophys. Res. Lett., 33, L10503, doi:10.1029/2006GL026075, 2006.
Wingham, D. J., Phalippou, L., Mavrocordatos, C., and Wallis, D.: The mean echo and echo cross product from a beamforming interferometric altimeter and their application to elevation measurement, IEEE Trans. Geosci. Remote Sens., 42, 2305–2323, 2004.
Zwally, H. J., Giovinetto, M. B., Li, J., Cornejo, H. G., Beckley, M. A., Brenner, A. C., Saba, J. L., and Yi, D.: Mass changes of the Greenland and Antarctic ice sheets and shelves and contributions to sea-level rise: 1992–2002, J. Glaciol., 51, 175, 509–527, 2005.

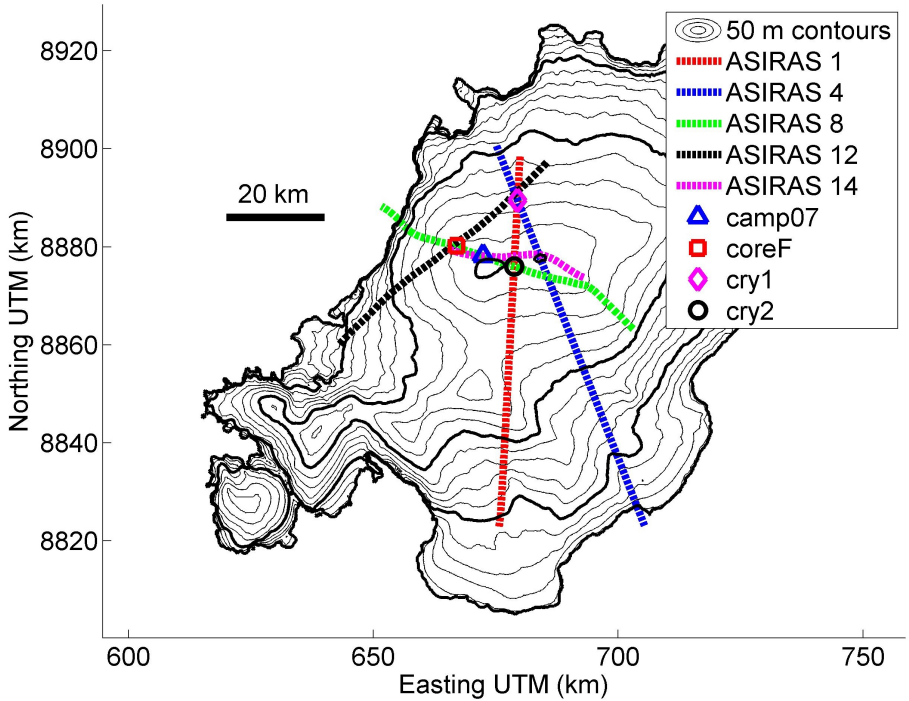

Fig. 1. Map of the Austfonna ice cap (bold contours show 250 m elevation intervals). ASIRAS ground tracks are shown together with the position of the four sites where ground-based VHB radar and snow and firn stratigraphy measurements were performed.

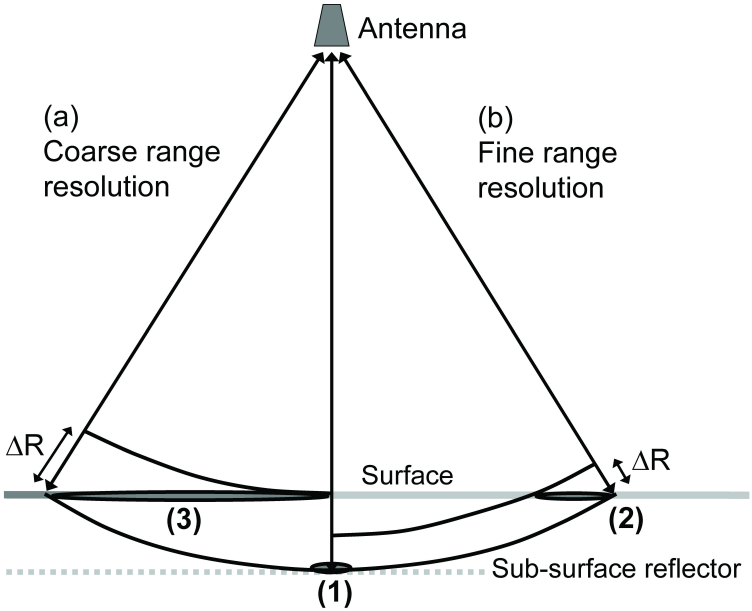

Fig. 2. Sketch showing how clutter from off-nadir reflectors can degrade a fine range resolution for nadir looking radars. In the case of a coarse range resolution (a), the off-nadir reflections (3) will merge with the lower reflector (1) in the same range bin. For a finer range resolution **(b)**, despite the range bin appearing to stem from only the subsurface when viewed in nadir, off-nadir returns (2) will still merge with the subsurface reflection (1) forming a convolved power at this range bin, degrading the range resolution.

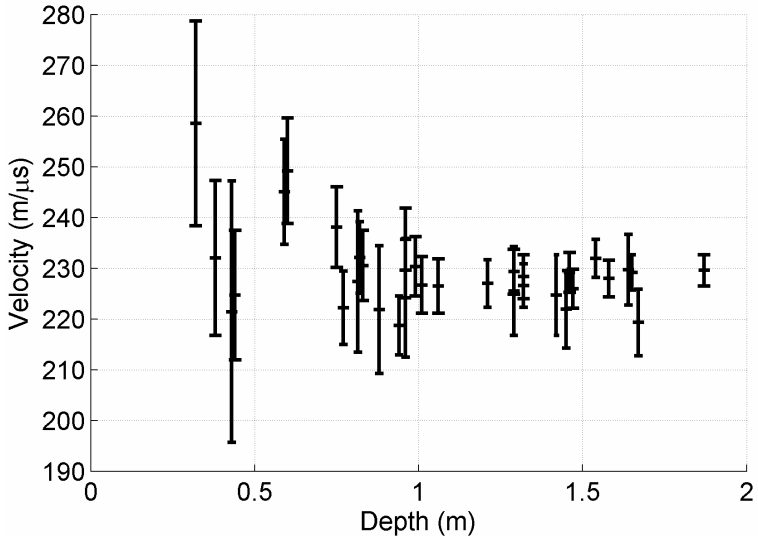

Fig. 3. EM-wave velocities calculated by inserting a metal reflector at various depths in the snow-pack.

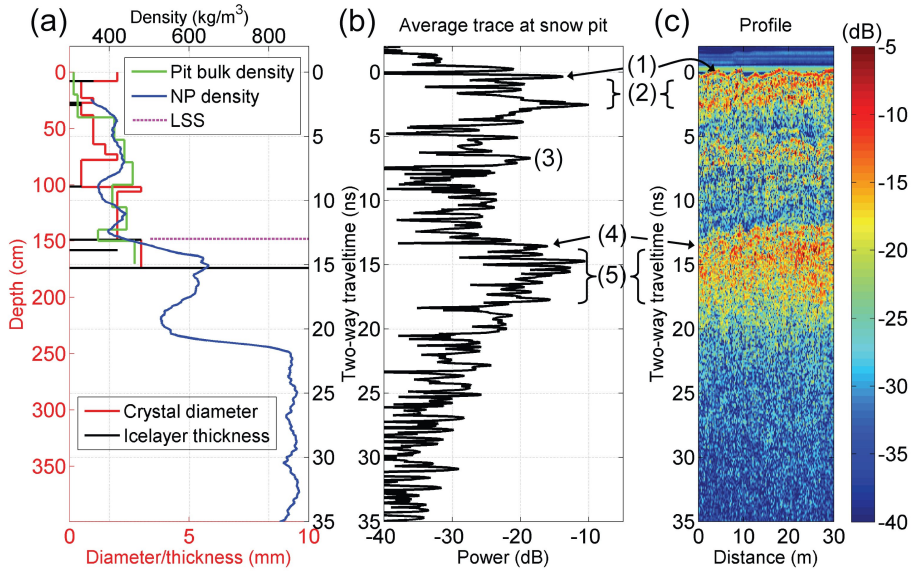

Fig. 4. Site "cry1": **(a)** ground-truth data, i.e. bulk density, typical crystal diameter, ice layer thickness, neutron probe profile and the position of the Last Summer Surface (LSS) (at 13 ns). The two-way travel time depth conversion is done using a speed of 2.28×10^8 m s^{-1} (Note the multiple y-axes). **(b)** average trace at the snow pit position (13.5 GHz center frequency and 8 GHz bandwidth). Numbers indicate features discussed in the text. **(c)** VHB profile extending from the snow pit, located at distance zero, along ASIRAS profile 1.

TCD
2, 777–810, 2008

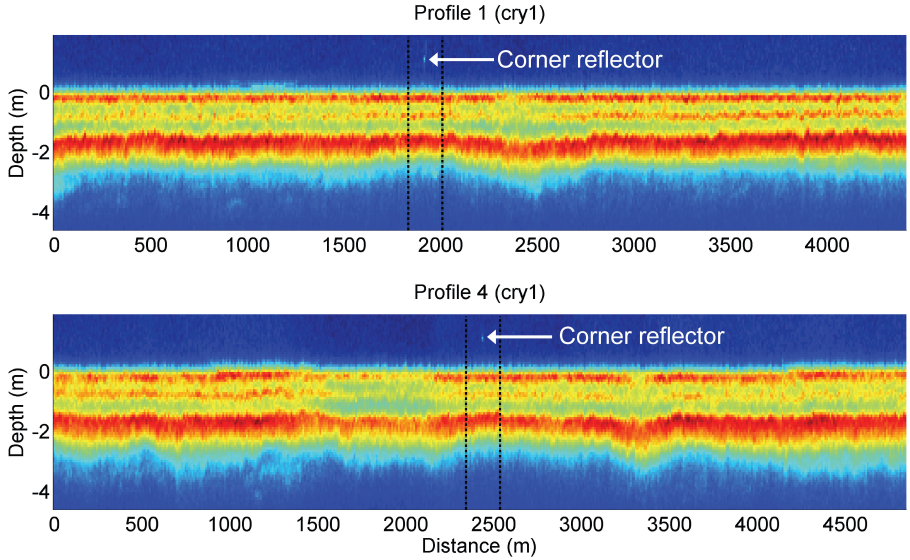

Fig. 5. ASIRAS data from site "cry1" (dB). Each profile comprises 500 traces. Due to variation in aircraft velocity, the length of the two profiles differs. The response of a corner reflector (~2 m above the surface) is marked by white arrow. Black dash-dotted lines shows the data used for direct comparison with the ground-based VHB radar data (Fig. 6). A wave velocity of 2.28×10^8 m s^{-1} has been used to convert two-way travel time to depth.

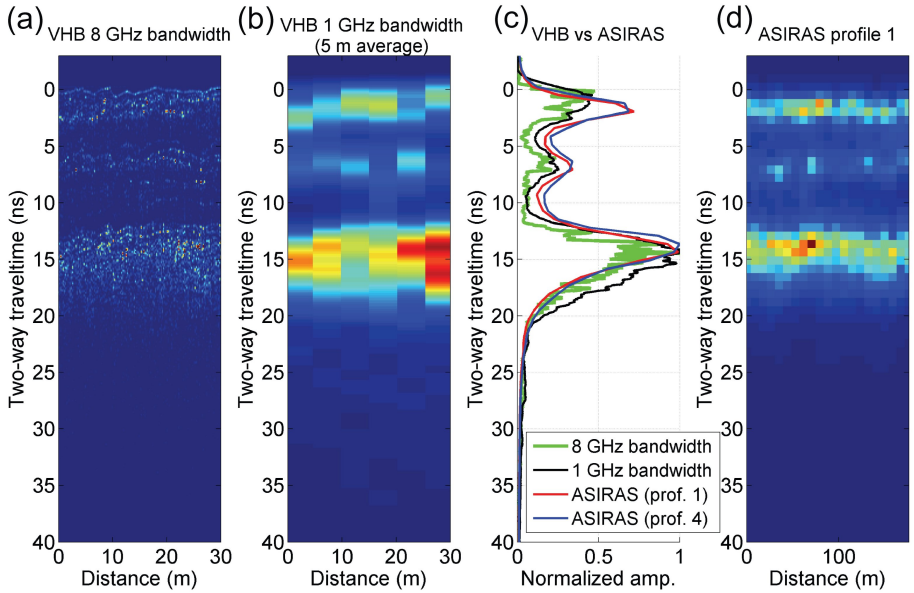

Fig. 6. **(a)** 8 GHz bandwidth ground-based VHB radar profile (power) at site "cry1". **(b)** Corresponding profile after reducing the bandwidth to 1 GHz and stacking to give 5 m average traces, more comparable to the ASIRAS 5×50 m footprint. **(c)** ASIRAS and VHB median traces (normalized) **(d)** ASIRAS intensity (power) along profile 1.

TCD
2, 777–810, 2008

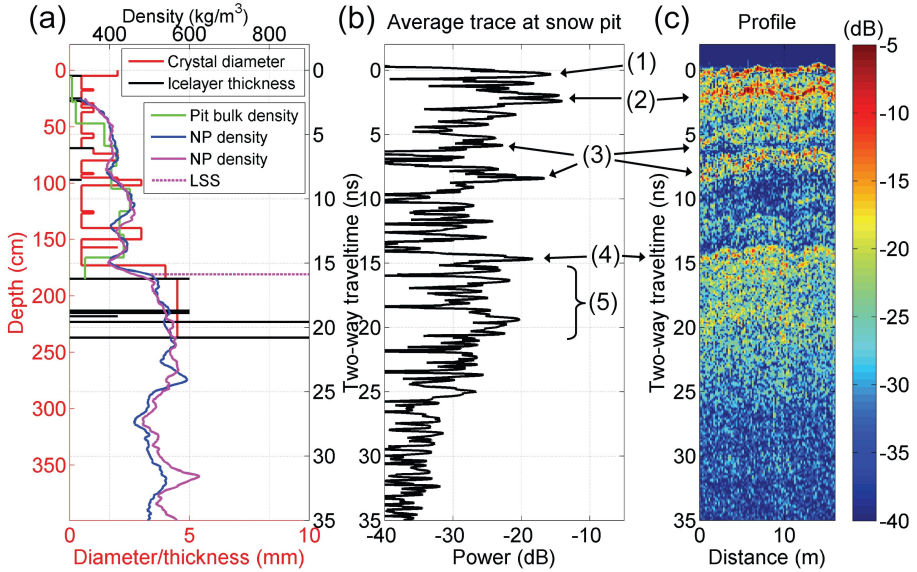

Fig. 7. Site "cry2": **(a)** ground-truth data i.e. bulk density, typical crystal diameter, ice layer thickness, neutron probe profile and the position of LSS (1.81 m). **(b)** Average trace at the snow pit position (13.5 GHz center frequency and 8 GHz bandwidth). Numbers indicate features discussed in the text. **(c)** VHB radar profile (snow pit located at distance zero).

TCD
2, 777–810, 2008

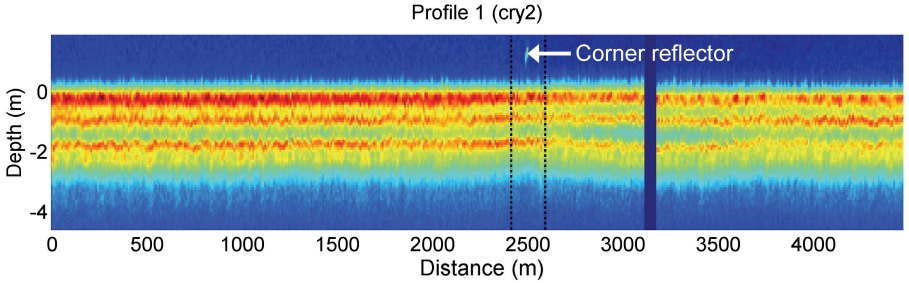

Fig. 8. ASIRAS profile 1 passing over site "cry2" (500 traces in dB format). The corner reflector is marked by white arrow. The traces used to compare to ground-based radar measurements (Fig. 9) are within the black dash-dotted vertical lines.

TCD
2, 777–810, 2008

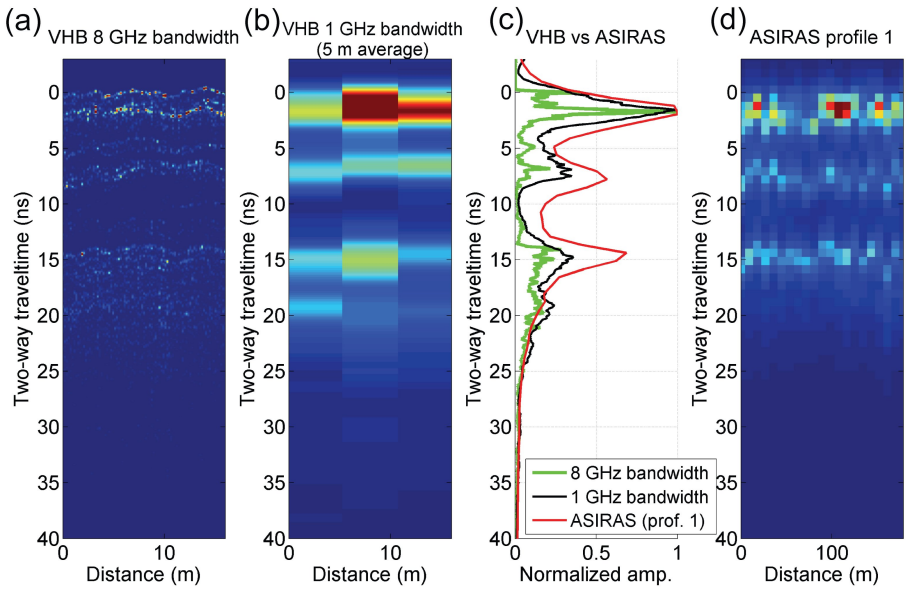

Fig. 9. **(a)** 8 GHz bandwidth ground-based VHB radar profile (power) at site "cry2". **(b)** Corresponding profile (5 m stacking) at 1 GHz bandwidth. **(c)** ASIRAS and VHB median traces (normalized) **(d)** ASIRAS intensity (power) format profile 1.

TCD
2, 777–810, 2008

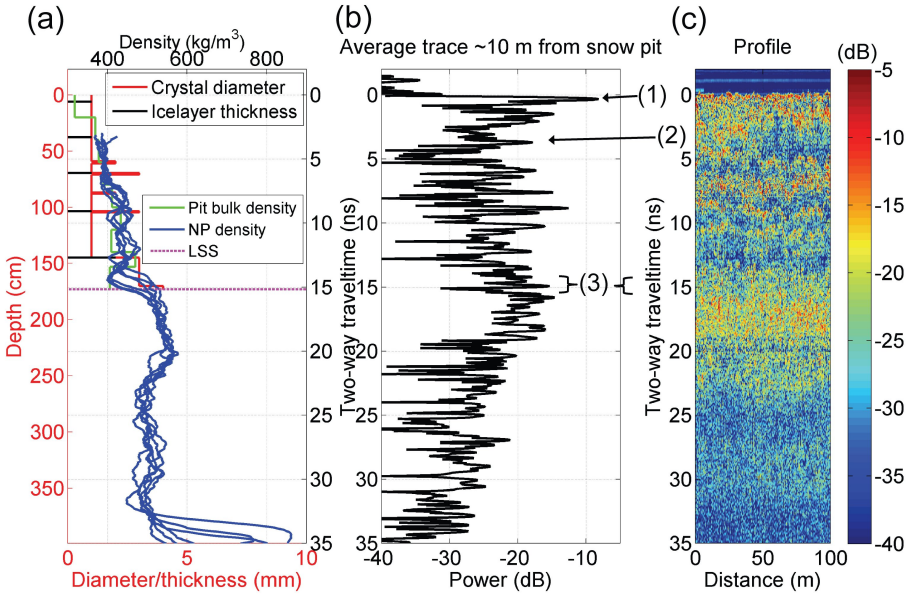

Fig. 10. Site "camp07": **(a)** ground-truth data i.e. bulk density, typical crystal diameter, ice layer thickness, neutron probe profile and the position of LSS (1.73 m). **(b)** Average trace at the closest position of the snow pit, ~5 m (13.5 GHz center frequency and 8 GHz bandwidth). **(c)** VHB profile. Note, the two low-backscatter bands at and just above 20 ns, are artifacts of removing an imperfectly matched background signal.

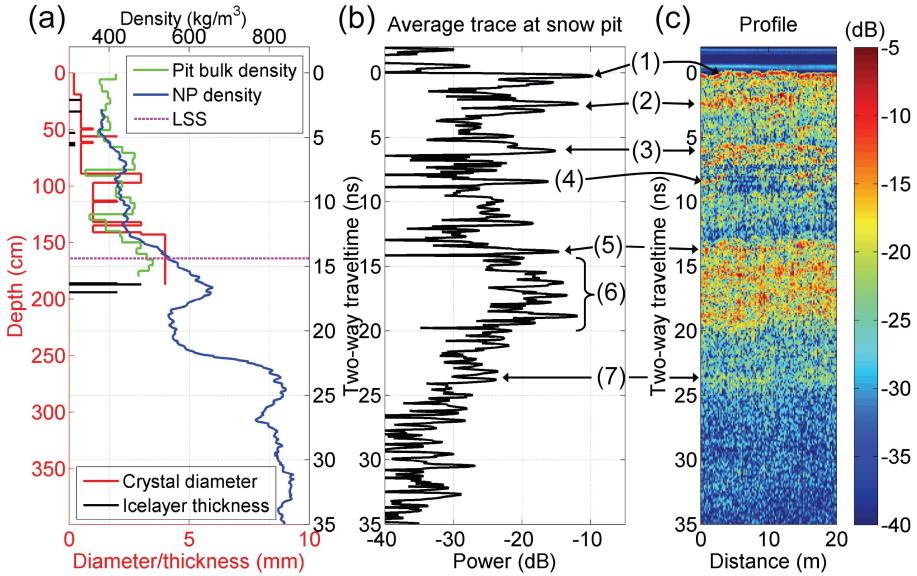

Fig. 11. Site "coreF": **(a)** ground-truth data i.e. bulk density, typical crystal diameter, ice layer thickness, neutron probe profile and the position of LSS (1.64 m). **(b)** Average trace next to the snow pit (13.5 GHz center frequency and 8 GHz bandwidth). **(c)** VHB profile extending out from the snow pit (located at distance zero).

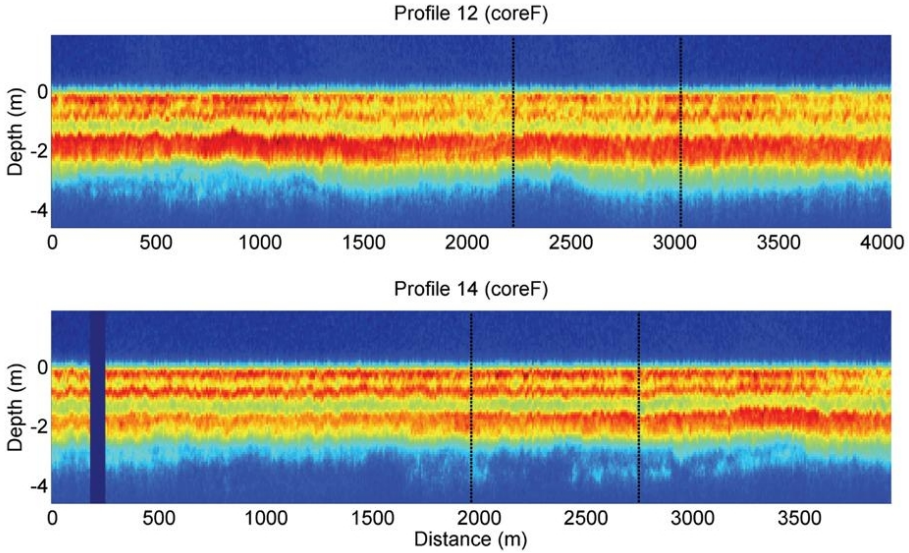

Fig. 12. ASIRAS data from the vicinity of the "coreF" site (dB). Each illustrated profile section comprises 500 traces, but vary in length due to different aircraft velocity. Dashed black lines shows the parts of the profiles closest to the ground site "coreF" (~800 m away).

TCD
2, 777–810, 2008